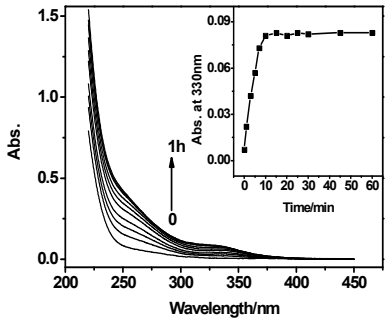

Figure S1. Time-dependent UV-vis absorption spectra in 10 mM KCl solution (pH 6.0) containing 7.20 μM rabbit liver apo-MT2 and 20 mol eq. of Pb^{2+}. The inset is the absorbance values at 330 nm plotted as a function of time.

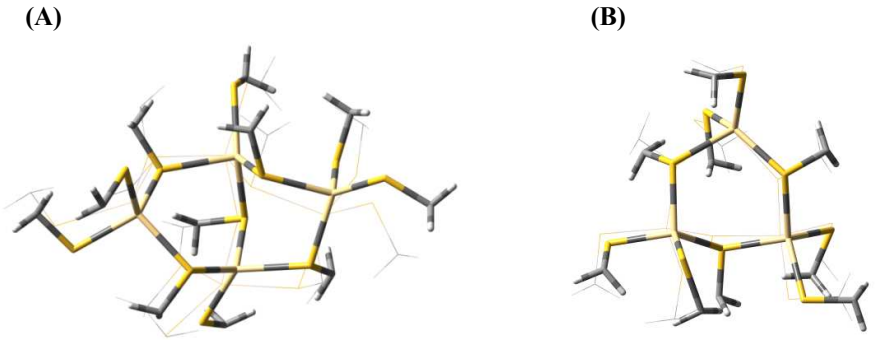

Figure S2. The structures of Cd_4–αMT2 (A) and Cd_3–βMT2 (B) from QM calculations. The thin line represents the structures in solution derived by NMR (from reference: *J. Mol. Biol.* 1988**,** *201*, 637-657).

Table S1. All Cd–S bond lengths in Cd_7-MT2 deduced from the ONIOM calculation.

	Bond length (Å) of Cd_4–αMT2			Bond length (Å) of Cd_3–βMT2	
	Exp. [1]	ONIOM calculation		Exp. [1]	ONIOM calculation
S1–Cd1	2.52	2.59	S12–Cd5	2.53	2.55
S2–Cd1	2.53	2.57	S13–Cd5	2.53	2.61
S3–Cd1	2.63	2.64	S14–Cd5	2.70	2.70
S4–Cd1	2.50	2.55	S15–Cd5	2.54	2.54
S2–Cd2	2.64	2.55	S2–Cd6	2.60	2.63
S5–Cd2	2.48	2.51	S5–Cd6	2.52	2.58
S6–Cd2	2.49	2.51	S6–Cd6	2.53	2.55
S7–Cd2	2.66	2.65	S7–Cd6	2.54	2.56
S3–Cd3	2.64	2.62	S3–Cd7	2.52	2.55
S7–Cd3	2.47	2.53	S7–Cd7	2.60	2.65
S8–Cd3	2.50	2.56	S8–Cd7	2.48	2.51
S9–Cd3	2.53	2.58	S9–Cd7	2.51	2.57
S4–Cd4	2.47	2.52	RMSD(d)	-	0.04
S9–Cd4	2.43	2.65			
S10–Cd4	2.69	2.60			
S11–Cd4	2.44	2.52			
RMSD(d)	-	0.05			

[1] Experimental data were from reference (*J. Mol. Biol.* 1988**,** *201*, 637-657).

Table S2. The S–Pb–S bond angles in Pb_7–MT2(I)

	Bond angle (deg)		Bond angle (deg)		Bond angle (deg)
S1–Pb1–S2	100.89	S2–Pb1–S3	89.50	S3–Pb1–S1	110.42
S4–Pb2–S5	96.20	S5–Pb2–S6	106.11	S6–Pb2–S4	97.30
S7–Pb3–S8	103.14	S8–Pb3–S9	103.60	S9–Pb3–S7	102.69
S10–Pb4–S11	96.65	S11–Pb4–S12	95.34	S12–Pb4–S10	88.25
S13–Pb5–S14	92.76	S14–Pb5–S15	100.09	S15–Pb5–S13	118.15
S16–Pb6–S17	112.60	S17–Pb6–S18	96.61	S18–Pb6–S16	96.63
S18–Pb7–S19	101.91	S19–Pb7–S20	94.74	S20–Pb7–S18	105.22

Table S3. Vertical excitation energies (in nm), oscillator strengths (f) and molecular orbital (MO) contributions involved in the electronic transitions of Pb_4–αMT2(I) for band at 330 nm calculated with the B3LYP functional.

$\lambda_{exp.}$ (nm)	$\lambda_{cal.}$ (nm)	Oscillator (f)	MO contribution (%)	
330	345.3	0.0045	HOMO→LUMO (93)	
	341.6	0.0071	HOMO-1→LUMO (96)	
	332.0	0.0159	HOMO-2→LUMO (62)	HOMO→LUMO+1 (34)
	326.4	0.0358	HOMO-1→LUMO+1(46)	HOMO-2→LUMO(25)
			HOMO-2→LUMO+1(12)	HOMO-3→LUMO (9)
	321.8	0.0175	HOMO-2→LUMO+1(62)	HOMO-2→LUMO(11)
			HOMO-3→LUMO+1(14)	HOMO-3→LUMO(7)
	308.4	0.0217	HOMO-3→LUMO+1(71)	HOMO-2→LUMO+1(12)
	298.0	0.0230	HOMO-4→LUMO (60)	HOMO-1→LUMO+3 (13)
			HOMO-4→LUMO+1(12)	HOMO-2→LUMO+2 (6)

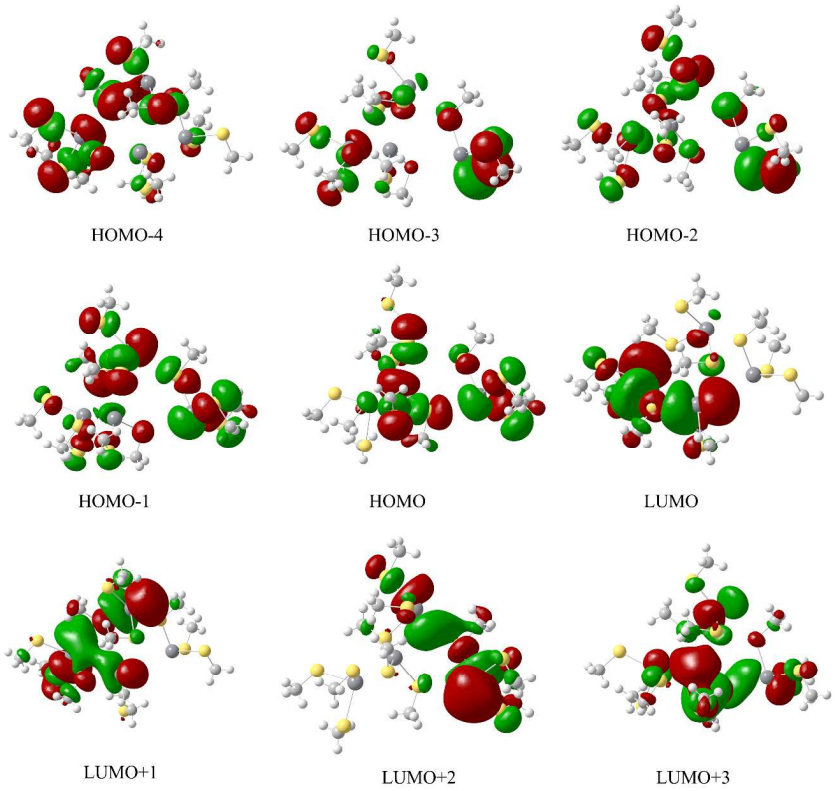

Figure S3. Typical frontier molecular orbitals (MO) responsible for the electronic transitions of Pb_4–αMT2(I) for band at 330 nm.

Table S4. The S–Pb–S and S–Pb–O bond angles in Pb_7–MT2(II)

	Bond angle (deg)		Bond angle (deg)		Bond angle (deg)
S1–Pb1–S2	97.49	S2–Pb1–O1	102.85	O1–Pb1–S3	87.75
S3–Pb1–S1	87.31				
S4–Pb2–S5	99.64	S5–Pb2–S6	100.16	S6–Pb2–S4	102.01
S7–Pb3–S8	92.33	S8–Pb3–S9	100.02	S9–Pb3–S7	106.76
S10–Pb4–S11	88.81	S11–Pb4–S12	99.57	S12–Pb4–S10	97.39
S13–Pb5–S14	115.04	S14–Pb5–S15	100.02	S15–Pb5–S13	91.82
S16–Pb6–O2	104.54	O2–Pb6–S17	92.65	S17–Pb6–S16	112.66
S18–Pb7–S19	99.50	S19–Pb7–S20	93.37	S20–Pb7–S18	110.92

Table S5. Vertical excitation energies (in nm), oscillator strengths (f) and molecular orbital (MO) contributions involved in the electronic transitions for three absorption bands of Pb_4–αMT2(II) calculated with the B3LYP functional.

$\lambda_{exp.}$(nm)	$\lambda_{cal..}$ (nm)	Oscillator (f)	MO contribution (%)	
400	408.9	0.0050	HOMO→LUMO (94)	
	406.8	0.0152	HOMO-1→LUMO (96)	
	400.8	0.0098	HOMO-1→LUMO+1 (71)	HOMO-1→LUMO (25)
375	383.2	0.0039	HOMO-1→LUMO+1(53)	HOMO-2→LUMO(25)
	378.9	0.0384	HOMO-1→LUMO(49)	HOMO-2→LUMO+1(27)
	375.5	0.0138	HOMO-2→LUMO+1(78)	HOMO-2→LUMO(12)
325	347.6	0.0145	HOMO-2→LUMO+2(65)	HOMO→LUMO+3(24)
	338.0	0.0121	HOMO-3→LUMO+2(62)	HOMO-1→LUMO+2(16)
	329.2	0.0498	HOMO-2→LUMO+3(63)	HOMO-2→LUMO+2(21)
	333.2	0.0498	HOMO-3→LUMO+3(57)	HOMO-2→LUMO+3(29)
	329.9	0.0469	HOMO-4→LUMO+3(48)	HOMO-3→LUMO+3(27)
	319.9	0.0103	HOMO-4→LUMO+3(49)	HOMO-2→LUMO+3(23)
			HOMO-2→LUMO+3(12)	HOMO-2→LUMO+2(7)

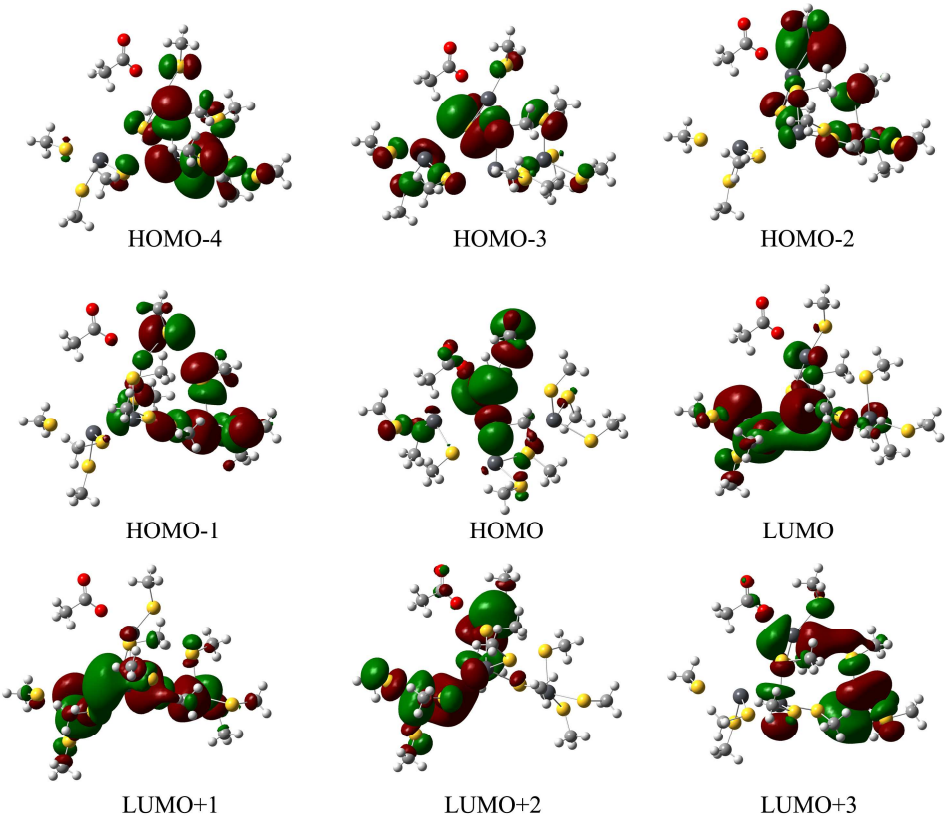

Figure S4. Typical frontier molecular orbitals (MO) responsible for the electronic transitions for three absorption bands of Pb_4–αMT2(II).

Table S6. The Pb–S bond lengths in Pb_7–MT2(I) by BP86

	Bond length (Å)		Bond length (Å)		Bond length (Å)
Pb1–S1	2.643	Pb1–S2	2.721	Pb1–S3	2.633
Pb2–S4	2.696	Pb2–S5	2.709	Pb2–S6	2.647
Pb3–S7	2.671	Pb3–S8	2.702	Pb3–S9	2.693
Pb4–S10	2.664	Pb4–S11	2.684	Pb4–S12	2.703
Pb5–S13	2.701	Pb5–S14	2.684	Pb5–S15	2.666
Pb6–S16	2.693	Pb6–S17	2.687	Pb6–S18	2.703
Pb7–S18	2.721	Pb7–S19	2.650	Pb7–S20	2.669

Table S7. The S–Pb–S bond angles in Pb_7–MT2(I) by BP86

	Bond angle (deg)		Bond angle (deg)		Bond angle (deg)
S1–Pb1–S2	101.21	S2–Pb1–S3	89.67	S3–Pb1–S1	109.43
S4–Pb2–S5	96. 02	S5–Pb2–S6	106.31	S6–Pb2–S4	98.50
S7–Pb3–S8	104.24	S8–Pb3–S9	104.60	S9–Pb3–S7	101.89
S10–Pb4–S11	96.75	S11–Pb4–S12	97.34	S12–Pb4–S10	89.22
S13–Pb5–S14	93.56	S14–Pb5–S15	99.05	S15–Pb5–S13	116.22
S16–Pb6–S17	111.21	S17–Pb6–S18	98.68	S18–Pb6–S16	97.36
S18–Pb7–S19	100.98	S19–Pb7–S20	95.24	S20–Pb7–S18	104.12

Table S8. The Pb–S and Pb–O bond lengths in Pb_7–MT2(II) by BP86

	Bond length (Å)		Bond length (Å)		Bond length (Å)		Bond length (Å)
Pb1–S1	3.089	Pb1–S2	2.846	Pb1–S3	2.793	Pb1–O1	2.456
Pb2–S4	2.740	Pb2–S5	2.682	Pb2–S6	2.739		
Pb3–S7	2.712	Pb3–S8	2.721	Pb3–S9	2.749		
Pb4–S10	2.723	Pb4–S11	2.718	Pb4–S12	2.749		
Pb5–S13	2.729	Pb5–S14	2.734	Pb5–S15	2.745		
Pb6–S16	2.857	Pb6–S17	2.834	Pb6–O2	2.267		
Pb7–S18	2.725	Pb7–S19	2.760	Pb7–S20	2.736		

Table S9. The S–Pb–S and S–Pb–O bond angles in Pb7–MT2(II) by BP86

	Bond angle (deg)		Bond angle (deg)		Bond angle (deg)
S1–Pb1–S2	97.53	S2–Pb1–O1	102.76	O1–Pb1–S3	87.85
S3–Pb1–S1	89.01				
S4–Pb2–S5	100.24	S5–Pb2–S6	99.86	S6–Pb2–S4	101.98
S7–Pb3–S8	92.93	S8–Pb3–S9	100.53	S9–Pb3–S7	108.66
S10–Pb4–S11	89.38	S11–Pb4–S12	100.88	S12–Pb4–S10	98.79
S13–Pb5–S14	116.54	S14–Pb5–S15	101.82	S15–Pb5–S13	92.02
S16–Pb6–O2	103.54	O2–Pb6–S17	91.65	S17–Pb6–S16	110.66
S18–Pb7–S19	99.90	S19–Pb7–S20	93.48	S20–Pb7–S18	110.78

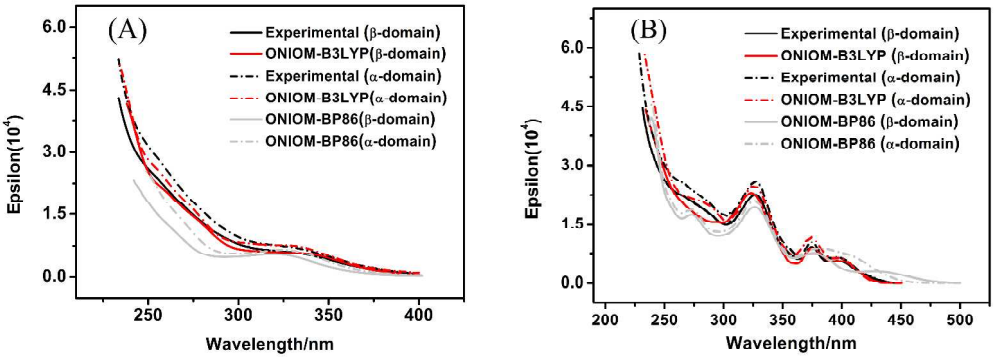

Figure S5. The electronic absorption spectra of individual domains in Pb_7–MT2(I) (A) and Pb_7–MT2(II) (B) obtained by B3LYP and BP86 functional, respectively.

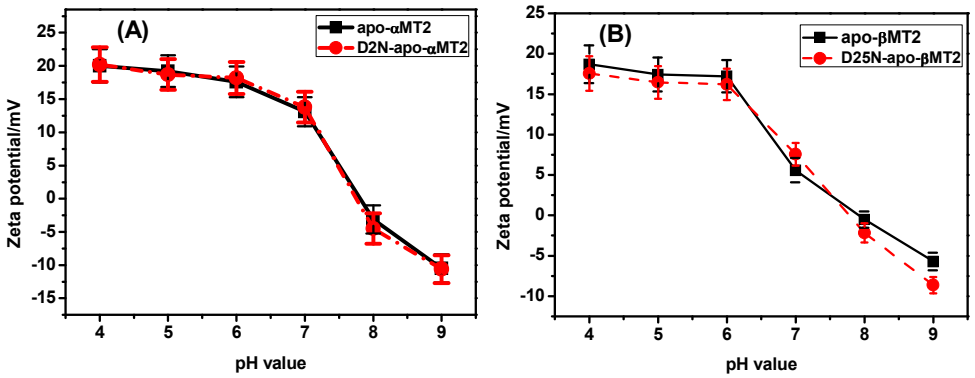

Figure S6. Zeta potentials of apo–αMT2 (panel A), apo–βMT2 (panel B) and the corresponding mutants. All the concentrations of the peptide solutions are 7.20 μM.

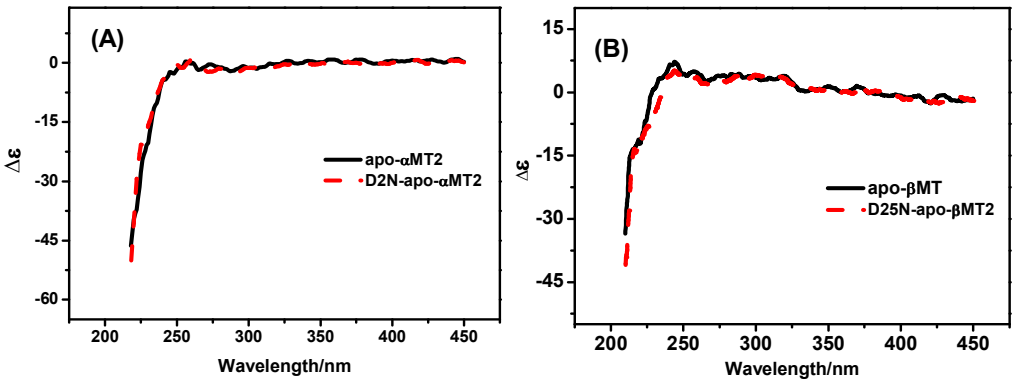

Figure S7. CD spectra of apo–αMT2 (panel A), apo–βMT2 (panel B) and the corresponding mutants. All the concentrations of the peptide solutions are 7.20 μM.

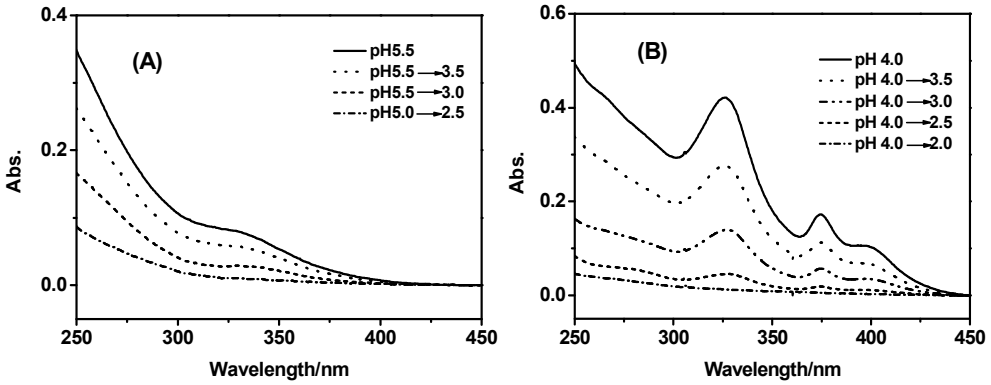

Figure S8. pH-dependent UV-vis absorption spectra of Pb_7–MT2(I) (A) and Pb_7–MT2(II) (B). The incubation time is 30 min.

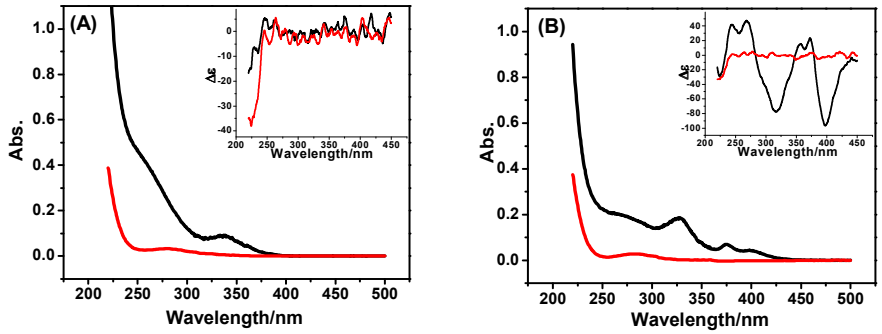

Figure S9. UV-vis absorption (A) and CD spectra (B) of 7.20 μM human apo-βMT2 in a KCl solution containing 20 mol eq of Pb^{2+}. The black curves are the results at pH 7.0, and the red curves are at pH 4.0.

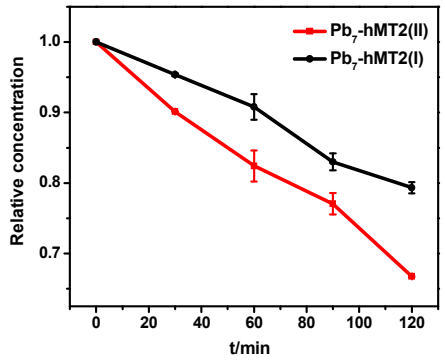

Figure S10. Time-dependent proteolytic processing of Pb_7–hMT2(I) (black curve) and Pb_7–hMT2(II) (red curve) by cathepsin B.